AIAA JOURNAL
Vol. 40, No. 4, April 2002

Modeling of Infrared Radiation in a Space Transportation System Environment

S. F. Gimelshein*
George Washington University, Washington, D.C. 20052
D. A. Levin†
Pennsylvania State University, University Park, Pennsylvania 16802
and
R. J. Collins‡
University of Minnesota, Minneapolis, Minnesota 55455

An approach for modeling the infrared (IR) glow radiation about the space shuttle at low-Earth-orbit flight altitudes is examined. The study builds on the modeling and numerical techniques developed for understanding the visible glow of the Atmospheric Explorer. Because of the rarefied nature of the flow, a direct simulation Monte Carlo method is used. The study extends the earlier gas-phase reaction model to include NO vibrational-state-specific formation using cross sections derived from quasi-classical trajectory calculations. IR spectra are computed using the state-specific NO vibrational levels and an accurate line-by-line spectral model. The effect of internal and translational energy accommodation coefficients in the Maxwell gas–surface interaction model was studied. The translational energy accommodation coefficient affects the width of the NO overtone transition ($\Delta\nu = 2$) spectral peak, and a value less than unity is required to give good agreement between modeling and experiment. The vibrational energy accommodation coefficient significantly impacts the magnitude of the NO infrared spectra. The influence of surface reactions on the IR spectra was also examined and shown to be small. Finally, simulated spectra are compared with IR data obtained from shuttle space flight experiments. The comparison shows that the postulated gas and gas–surface phase models used in particle simulation enable one to predict quantitatively IR spectra at high altitudes.

I. Introduction

SPACECRAFT glow is caused by the interaction of spacecraft surfaces with the rarefied atmosphere in low Earth orbit. Detailed information on the physical and chemical processes that occur at the surface and in the gas phase is critical for understanding glow formation mechanisms and for interpretation of the experimental data obtained in recent years.[1,2] Numerical methods that enable one to model spacecraft glow are of great importance because they can provide for very detailed information on the spacecraft local atmosphere, which can affect onboard optical sensors. However, accurate models for gas-phase and gas–surface collision processes need to be employed to improve the credibility of numerical predictions.

Because spacecraft glow processes occur at high altitudes, traditional computational fluid dynamics approaches fail, and methods of rarefied gasdynamics have to be used. The most successful method of rarefied gasdynamics for modeling chemically reacting flows is the direct simulation Monte Carlo (DSMC) method, which can be applied for the simulation of two- and three-dimensional chemically reacting flows about space vehicles in the transitional regime. Reliable results require the use of accurate and adequate models for gas-phase and gas–surface collision processes. An approach for modeling surface processes has been developed in Refs. 3–5, suitable for the DSMC method. The DSMC approach presented in these papers improves the efficiency of the computational procedure so that sufficient accuracy can be obtained at all altitudes of interest. Moreover, this high accuracy permits us to evaluate the sensitivity of predicted radiation to changes in freestream conditions, chemistry models, surface models, and radiation. Many of these comparisons involve small differences; hence, high accuracy is a necessity.

The process responsible for glow in the visible portion of the spectrum[2,6] is the emission from NO_2^* molecules (where NO_2^* denotes an excited electronic state of NO_2) formed by the recombination of atmospheric, hyperthermal $O(^3P)$ atoms with surface-adsorbed NO. The principal process for surface glow follows an Eley–Rideal mechanism (see Ref. 7) with NO_2^* formed by subsequent collisions of O with surface-physisorbed NO. The DSMC modeling of Collins et al.,[5] Karipides et al.,[8] and Gimelshein et al.[9] showed that there was sufficient NO formed in the diffuse bow shock to account for the NO_2^*-originated visible radiation measured by photometers onboard the Atmospheric Explorer (AE) spacecraft.[1] Hence, gas-phase NO, formed by the exchange reaction

$$N_2 + O \rightarrow NO + N \tag{1}$$

was demonstrated to be the glow precursor species.

Although there is a large body of glow radiance data from the shuttle, AE was selected for our initial modeling efforts because it was free of potential thruster firing surface contamination. Unlike the shuttle, however, AE did not obtain spectroscopic data and the spectral region of its photometers was limited to the visible and near-UV. Comparison of the experimental data obtained in the Spacecraft Kinetic Infrared Test (SKIRT),[10–12] flown on the shuttle with modeling, provides an opportunity to identify the state of the NO glow precursor.

This paper utilizes the previous findings while concentrating on a new aspect, the infrared glow radiation of vibrationally excited NO. The two major mechanisms influencing the formation of NO species will be studied. The first is the NO production in the gas phase by the exchange reaction given in Eq. (1). The second is the influence of the shuttle surface to the NO infrared (IR) spectra. There are two types of NO molecules that radiate in the field of view of the spectrometer, those that radiate before and after encountering the surface. Hence, by comparison with the NO IR measurements, we will be able to access our ability to model the visible glow precursor

Received 15 September 2000; revision received 29 March 2001; accepted for publication 1 October 2001.

*Senior Research Scientist, Department of Chemistry.
†Associate Professor, Department of Aerospace Engineering. Senior Member AIAA.
‡Professor Emeritus, Department of Electrical Engineering. Member AIAA.

species and the level of surface accommodation. The computational efforts of the work will be directed toward modeling of IR emission produced during the flight of the Space Transportation System at the orbit altitude of 263 km. The IR spectral radiation from NO in the wavelength range 1.5–5.5 μm as measured by the SKIRT instrument will be examined. Analysis of the SKIRT spectral data by Ahmadjian et al.[12] showed that the data are characterized by an NO vibrational temperature of approximately 8000 K.

The outline for the paper is as follows. The thermochemical and surface models used in earlier work will be presented. The salient features of the SMILE DSMC code and the NEQAIR-IR radiation models will be discussed. In the Results section, we show the sensitivity of the IR spectra to the degree of wall accommodation, the impact of surface reactions, and energy redistribution. Finally, comparison of theory with the SKIRT experimental data will be presented.

II. Thermochemical Model

A. Interactions with the Surface

Different gas–surface interaction models will be considered in this paper. The baseline case will consider the gas–surface interaction defined by use of the accommodation coefficients. In the baseline calculations, a Maxwell model is used for a nonreactive gas–surface interactions that assumes complementary fractions of diffuse and specular reflections for molecular translational and internal energies. Generally, the Maxwell model is constructed on the assumption that a fraction $1-\alpha$ of the molecules is reflected from the surface in a specular fashion, whereas the fraction α is reemitted diffusely, with the Maxwellian distribution. The words specular reflection are usually used for molecular velocities. Here, for convenience, we also apply them to the internal energies, implying that specular means no change of energies after a collision with a surface. In this work, the translational energy accommodation coefficient α_t is taken to be either 1 or 0.8. The vibrational energy accommodation coefficient α_v is varied from zero to one, and the rotational energy accommodation coefficient α_r is set equal to α_v. Note that it was found in Ref. 13 that for high-temperature nitric oxide $\alpha_t > \alpha_v > \alpha_r$. Because the IR spectra were determined to be least sensitive to the rotational energy accommodation coefficient, the relation $\alpha_v = \alpha_r$ was employed to avoid using α_r as one more free parameter. In this model, the wall is assumed to have no influence on the residence time of the incident gas flux species.

As was shown in earlier work, however, high-altitude gas–surface interactions that weakly bond NO to the spacecraft surface for a finite time are required to model the density dependence of the visible glow as well as its magnitude. Therefore, for the second and third surface models considered here, chemical reactions on the surface are included as the two limiting cases of surface parameters given in Table 1.

The detailed description of gas–surface high-altitude processes of the second and third surface models has been given in earlier work.[4] Briefly, the major surface processes responsible for the visible glow from NO_2^* are

$$NO + S \longleftrightarrow NO_S \tag{2}$$

$$O + NO_S \longrightarrow NO_2 + S + h\nu \tag{3}$$

$$M + NO_S \longrightarrow M + NO + S \tag{4}$$

Table 1 Summary of surface glow parameters

Parameter	Range of values
NO heat of absorption	16 kcal/mole[a] 20 kcal/mole[b]
O heat of absorption	3 kcal/mole
Sticking coefficients for adsorption processes	0.5
Wall temperature T_w	300 K
Glow cross sections for process (3)	0.1 Å^2
Scrubbing cross sections for process (4)	0 Å^2[a] 4 Å^2[b]
Total number of surface sites per square meter, n_T	0.24×10^{20}

[a]Second surface model. [b]Third surface model.

where S represents a surface site available for physisorbtion and NO_S represents that species adsorbed to the surface. Reactions (2), (3), and (4) are adsorption/desorption, glow processes, and scrubbing reactions, respectively. Equations (3) and (4) are assumed to proceed only in forward direction. The scrubbing processes involve all gas species (denoted as M), that is, N_2, O_2, NO, N, and O.

The desorption rate constant [reverse processes of Eq. (2)] is assumed to be temperature-dependent as $k\theta_D/h \exp(-H_s/kT_w)$, where H_s is the heat of absorption, k is the Boltzmann constant, θ_D is the Debye temperature, and T_w is the wall temperature. The forward rate is derived from the inherent properties of the gas species incident on the surface and the surface material by use of the sticking coefficient. Table 1 gives the values of the surface parameters[5] that were used in this work for the second and third surface models.

B. Gas-Phase Chemical Reactions and Vibrational Energy Redistribution

A seven-species mixture consisting of N, O, N_2, O_2, NO, NO_2^*, and NO_2 was used. At the high altitudes studied, the impact of chemical reactions on major species N_2, O_2, and O, is negligibly small. Only the reaction path, Eq. (1), may, therefore, affect the formation of NO_2^*. In previous work, we used the conventional total collision energy (TCE) model (see Ref. 14) and a model based on the reaction cross sections obtained through the trajectory calculations of Bose and Candler.[15] We found the second model to provide a higher yield of NO formation for the AE conditions.[3] In this work, we only use the Bose and Candler[15] cross-section data. In addition, because our goal is to model accurately the NO IR spectra, we treated each vibrational level of NO (up to 21 levels) as a separate flow species. For a given precollision N_2–O relative energy, the Bose and Candler[15] vibrational–rotational state-specific cross sections were assumed to follow a Boltzmann distribution in terms of the postcollisional vibrational and rotational energies of NO, as described in a private communication with D. Bose in December 1999.

Use of the quasi-classical (QC) cross-section data avoids the choice of a semi-empirical vibrational redistribution model such as that based on the Larsen–Borgnakke (LB) energy redistribution technique[16] or proportional energy partitioning.[17] However, accurate potential energy surfaces for chemical reactions are not usually available, and these phenomenological models must be used. To understand the difference between the QC model and a phenomenological model, the NO vibrational populations and resultant spectra based on both types of models will be compared. The LB technique of energy partitioning applied to the case of chemical reactions was the phenomenological approach used in this work. In this scheme, the energy between two energy modes (or, in the general case, sets of modes) a and b is calculated using the joint distribution function

$$f_e(E_a, E_b) = f_e(E_a) f_e(E_b)$$

where E_a and E_b are energies of modes a and b and f_e are equilibrium distribution functions

$$f_e(E) \propto E^{\xi/2-1} \exp[E/(kT)]$$

Here, ξ is the number of degrees of freedom of the corresponding mode. The energy E_a is then sampled from

$$f_e(E_a) f_e(E_c - E_a)$$

where E_c is the total energy of two modes (it does not change in a collision) and E_b is calculated as $E_c - E_a$. This routine is applied subsequently to redistribute the energy available after reaction over the reaction products and their modes. The phenomenological approach is similar to the LB model originally developed to model the energy transfer between translational and internal modes.

In the reaction of interest, $N_2 + O \rightarrow NO + N$, the procedure is as follows. First, the total energy of the system $N_2 + O$ is changed $E_c' = E_c + Q_{\text{reac}}$, where Q_{reac} is the reaction heat. Then, the energy E_c' is redistributed between the relative translational and internal NO modes. The relative translational energy is calculated using the joint distribution function

$$f_e(E_{\text{tran}}) f_e(E_c' - E_{\text{tran}})$$

and $E_{\text{int,NO}} = E_c' - E_{\text{tran}}$. Finally, $E_{\text{int,NO}}$ is redistributed between rotational and vibrational modes of NO. That means that the rotational energy is sampled from

$$f_e(E_{\text{rot,NO}})\, f_e(E_{\text{int,NO}} - E_{\text{rot,NO}})$$

and the vibrational energy is $E_{\text{vib,NO}} = E_{\text{int,NO}} - E_{\text{rot,NO}}$.

III. Numerical Methods

The SMILE computational tool based on the DSMC method will be used in computations; details may be found elsewhere.[18] The SMILE capabilities important for the present work are the accurate collision schemes, models for energy transfer, two-level rectangular grids adaptive to flow gradients, different grids for collisions and macroparameters, and parallel implementation with efficient load balancing techniques. The majorant frequency scheme is employed for modeling molecular collisions.[19] The variable hard sphere model was used for modeling intermolecular interactions. The LB model with temperature-dependent rotational and vibrational relaxation numbers was utilized for rotation–translation and vibration–translation energy transfer. The TCE model was employed to calculate all gas-phase chemical reactions except Eq. (1), for which the QC results were used. The complete list of reactions may be found elsewhere.[3]

SMILE was modified to account for surface reactions. Instead of a three-step approach used for modeling trace species gas-phase and surface reactions,[5] a more efficient one-step algorithm[4] was utilized. A weighting scheme[3] has been used to simulate both the elastic collision processes between major and trace species and the chemical reactions in gas phase and on the surface. The use of a weighting procedure is indispensable for obtaining credible results involving radiative processes due to the very small relative concentrations of species important for radiation. The procedure enables one to increase substantially the sample size of the trace species.

The radiation can be calculated by the use of the steady-state DSMC flow solution, which provides a two-dimensional spatial distribution of species concentrations and temperatures. For high-altitude conditions, it was assumed that the radiation was optically thin. The NEQAIR-IR model of Packan et al.,[20] an accurate line-by-line spectroscopic model, was used. The spectroscopic transitions appropriate to NO and OH in the spectral region from 1.0 to 7.5 μm were calculated under the assumption of either a Boltzmann distribution of vibrational states or the state-specific populations given by the QC or the LB model. For all cases, a Boltzmann distribution for the rotational temperature was assumed. The spectra were calculated with a spectral resolution of 0.1 Å and averaged over 600 Å, which approximates the circular variable filter (CVF) resolution of the SKIRT instrument of $\Delta\lambda/\lambda = 2\%$.

IV. Flow Conditions, Geometry, and Computational Parameters

The rarefied flow about the space shuttle at the altitude of 263 km was investigated. The freestream conditions used are listed in Table 2. The wall temperature is not known from experiment, and a constant value of 300 K commonly used for high altitudes is assumed hereafter. To determine the possible influence of the surface temperature on the IR spectra, a calculation was also performed at a surface temperature equal to 1100 K. The flow was simulated as two dimensional, with the geometrical setup given in Fig. 1. The

Table 2 Freestream conditions

Parameter	Value
Altitude	263 km
Speed	7922 m/s
Ambient temperature	1132 K
Total number density	$2.11e+15$ mol/m^3
Freestream mole fractions	
N_2	0.285
O_2	0.0128
O	0.65985
NO	0.00005
N	0.0423

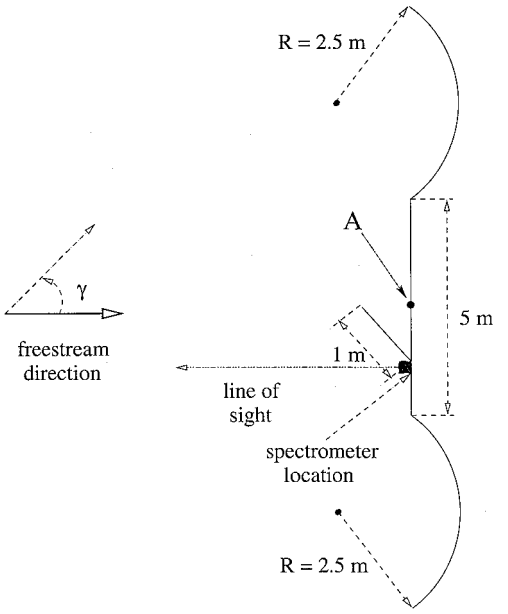

Fig. 1 Schematic of SKIRT shuttle measurements.

calculations were performed for two angles of attack, $\gamma = 0$ and 45 deg. Figure 1 also shows a schematic of the geometry of the SKIRT measurements onboard the shuttle.

The computational domain used in the calculations was from -65 to 5 m in the X direction [parallel to the line of sight (LOS)] and from -30 to 30 m in the Y direction, with the center of coordinates located in point A. (Contour level figures shown in the next section conform to these computational domain dimensions.)

A two-level grid was used to model the glow formation off of a flat plate in the field of view of the spectrometer. The average number of particles used to model the flow was about 420,000. The cell size for background cells in the collisional grid was 1×1 m, with a finer mesh of 10×10 cm used close to the body. This resulted in a total of approximately 70,000 collisional grid cells. The cell size in the macroparameter grid was 25×25 cm with a finer resolution of 5×5 cm used near the body. The total number of cells used in the macroparameter grid was approximately 85,000 cells. Note that the freestream mean free path at 260 km is of the order of 1000 m, which certainly makes the cell size appropriate from the point of view of DSMC requirement that cell size be smaller than the mean free path.

V. Computational Results

A. Influence of Energy Redistribution

Consider first the sensitivity of our simulations to the method of postcollisional vibrational energy redistribution. A translational energy accommodation coefficient of one was assumed, and two values of zero and one were used for the internal energy accommodation coefficients $\alpha_r = \alpha_v$.

Figures 2 and 3 show vibrational population distributions at a point close to the surface for the two redistribution models considered and the two limiting cases of vibrational energy wall accommodation. The resolution of the higher vibrational population states is challenging because they become a smaller fraction of NO, itself a trace species. Hence, if emphasis is given to the distributions up to level 10, we can deduce the following results from Figs. 2 and 3. For both internal energy accommodation coefficients, the QC calculations produce an NO population of levels smaller than seven, slightly higher than that for the LB energy redistribution approach, whereas the population of levels greater than seven is lower for the QC model.

Generally, the postcollision vibrational state distribution given by the QC data need not follow the LB energy redistribution because the QC results are determined by the reaction potential energy surface. In the absence of QC data, the total collision energy model and the LB model would typically be used. In our case, it was found that the

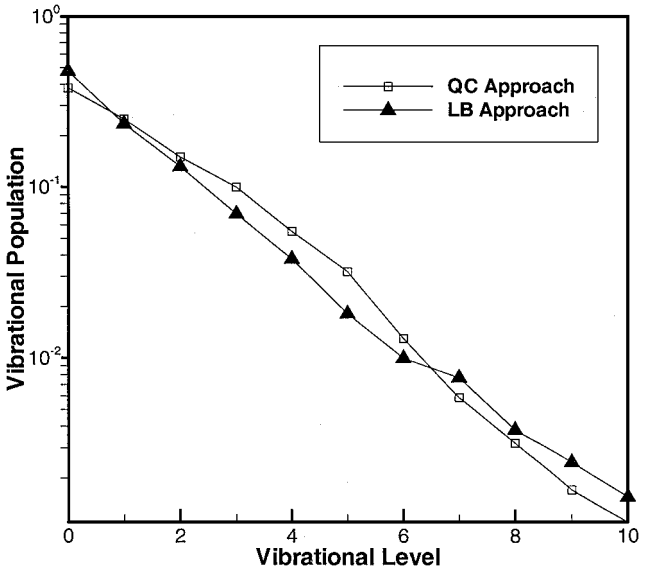

Fig. 2 Relative vibrational population distributions at $X = 0.1$ m along the LOS for the QC and the LB redistribution models; $\alpha_v = 0$ ($\alpha_t = 1$).

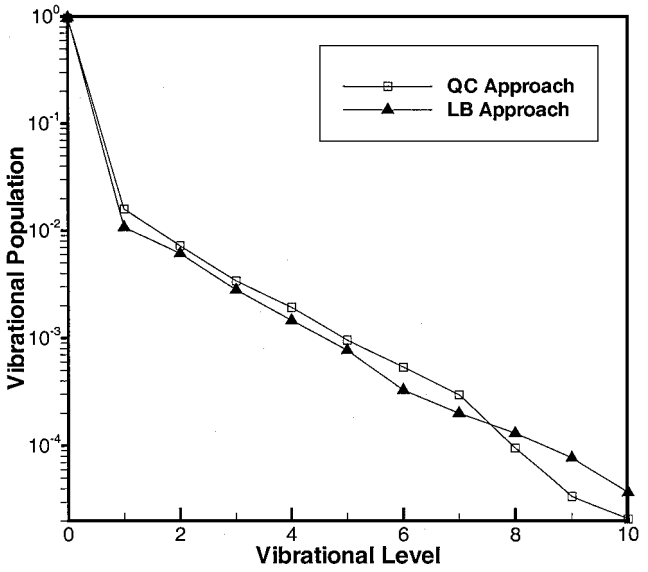

Fig. 3 Relative vibrational population distributions at $X = 0.1$ m along the LOS for the QC and the LB redistribution models; $\alpha_v = 1$ ($\alpha_t = 1$).

LB scheme enables one to obtain vibrational populations close to those produced with the QC model. The reason for that is that the QC model for reaction (1), under the conditions of interest, essentially follows the local equilibrium distribution of collision energy over the reaction products. This conclusion agrees with the results of Ref. 21, where the two models were compared in detail for several temperature conditions; however, this cannot be generally assumed for other reactions.

Figures 4 and 5 show the resultant spectra for the two energy redistribution models and limits of wall accommodation. Consistent with Figs. 2 and 3, the magnitude of the spectral radiance shown in Fig. 4 (no accommodation) is higher than for full accommodation (Fig. 5). When the two models of energy redistribution are compared, the QC model results give higher values of the radiation. The LB and QC energy redistribution models with and without accommodation give essentially the same width of the spectral distribution.

B. Macroparameter Flowfields and Sensitivity to Vibrational Accommodation Coefficient

The results shown in this subsection are for $\alpha_t = 1$, no surface reactions, different vibrational accommodation coefficients, and rotational and vibrational energy redistribution of NO formed by reaction (1) as given by the data of Bose and Candler.[15]

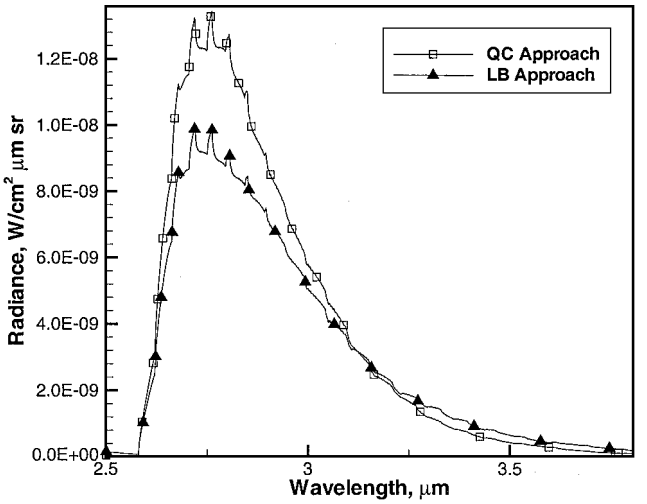

Fig. 4 Calculated spectra showing the NO IR overtone transition $\Delta\nu = 2$ and higher for two models of vibrational energy partitioning; $\alpha_v = 0$ ($\alpha_t = 1$).

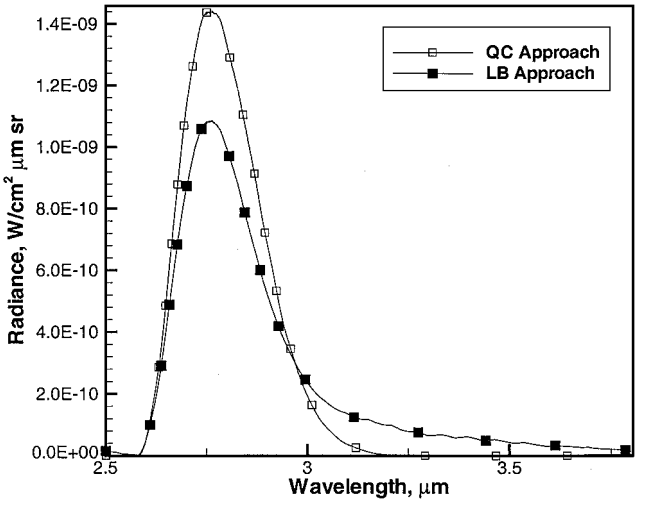

Fig. 5 Calculated spectra showing the NO IR overtone transition $\Delta\nu = 2$ and higher for two models of vibrational energy partitioning; $\alpha_v = 1$ ($\alpha_t = 1$).

Figure 6 presents the distribution of the total number density in the flow for $\alpha_v = 0$. Because the flow is highly rarefied, there is no clearly formed bow shock, and the density increases monotonically from the freestream boundary downstream to the surface. Note that the calculations were performed for larger computational domain sizes than shown here. The results were found to be insensitive to the increase of the domain. The total number density spatial distribution for fully diffuse accommodation on the surface, $\alpha_v = 1$, was found to be essentially the same. Similarly, Fig. 7 shows that the profile of NO number density along the LOS (see Fig. 1) is also almost independent of the degree of rotational–vibrational surface accommodation. This is reasonable because the main source of energy to create the diffuse shock and produce NO is due to the conversion of translational energy into chemical energy, and collisions with the translation–internal energy exchange are very rare in such a rarefied flow.

However, when one considers the dependence of the vibrational temperature distribution in the shock layer as a function of vibrational accommodation, the difference is much more dramatic. The NO vibrational temperature was determined from the following relationship:

$$\bar{\varepsilon}_{\text{av}} = \frac{k\theta_v}{\exp(\theta_v/T_v) - 1} \tag{5}$$

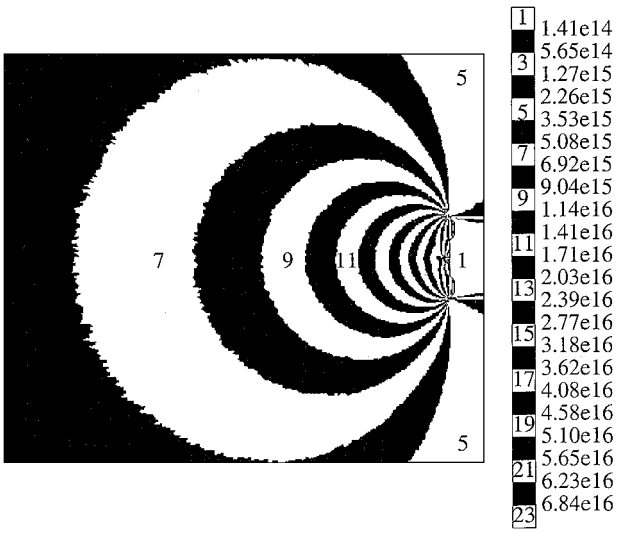

Fig. 6 Total number density contours levels in molecules per cubic meter for $\alpha_v = 0$.

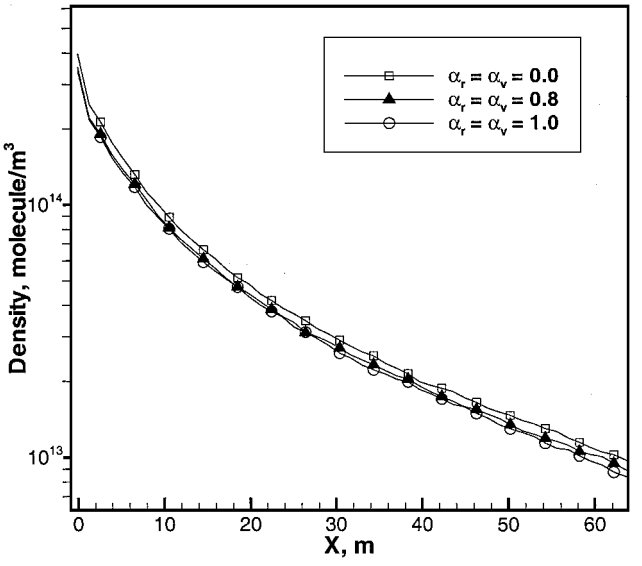

Fig. 7 NO number density along the LOS from the shuttle body to the freestream.

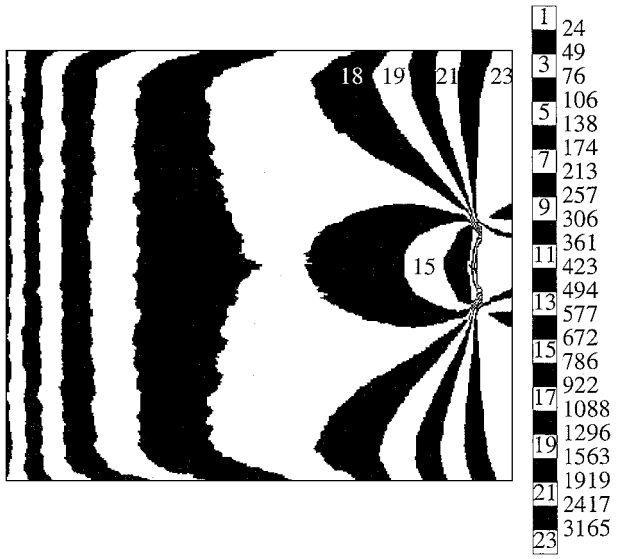

Fig. 8 Vibrational temperature contours for full accommodation with the surface, $\alpha_v = 1$, and the QC data.

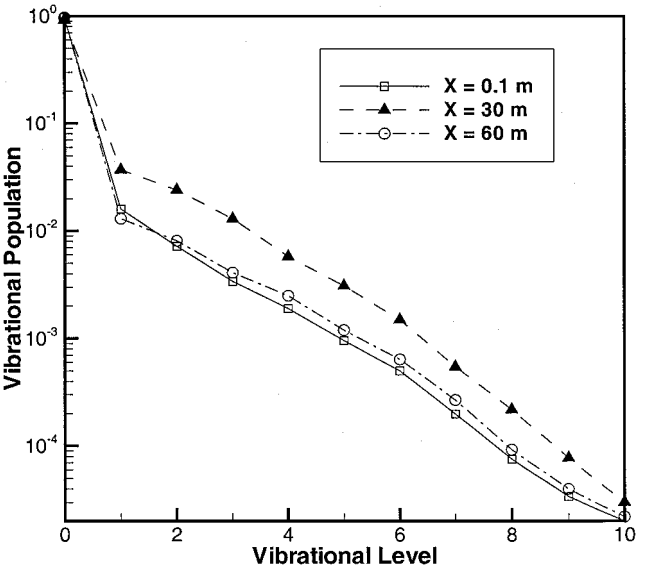

Fig. 9 Relative vibrational population distributions at three locations along the LOS for full accommodation with the surface, $\alpha_v = 1$, and the QC data; $X = 0.1$ m curve represents a point closest to the surface. The ordinate gives the fraction of NO molecules in the ν vibrational state relative to the total number of NO molecules at the indicated location.

where $\bar{\varepsilon}_{\text{av}}$ represents the cell averaged vibrational energy per particle and θ_v is the characteristic temperature of vibration. Figure 8 shows the spatial distribution of the NO vibrational temperature obtained for $\alpha_v = 1$. In contrast, the temperature field for no accommodation with the wall, $\alpha_v = 0$, is constant with a value of ~5000 K.

Figure 9 provides an alternative view of the NO vibrational temperature distributions at three distinct points along the LOS for full accommodation with the wall. The fraction of NO molecules in a given vibrational state ν is shown as a function of vibrational level at each of the three locations. Note that, for $\nu > 1$, all three locations exhibit the same dependence that can be characterized by a temperature of ~5000 K. However, when the $\nu = 0$, 1 levels are considered, the vibrational states do not follow a Boltzmann distribution, and the variation in vibrational temperatures shown in Fig. 8 is due to the large change in slope introduced by these two states. The change in population distributions is not uniform as we progress from a location close to the body ($X = 0.1$ m) toward the freestream (60 m). This is because there are three sources of NO in the flowfield: freestream (~10%) NO and NO chemically formed that either has collided or has not collided with the surface. For the location closest to the surface, the majority of the NO is formed chemically and collided with the wall, whereas at 30 m, the fraction of NO molecules that did not collide with the wall is higher. At 60 m, most of the NO is from the relatively cooler freestream. Note from Fig. 9 that the vibrational state distribution at 30 m is the highest. This is consistent with the concept that the highest vibrational distribution occurs during the gas-phase NO formation process, and collisions with full accommodation lower the vibrational energy.

If we select a point in the flow (for example, close to the body at $X = 0.1$ m), we can consider the change in vibrational state distribution for a variable vibrational accommodation coefficient. Figure 10 shows the vibrational state distribution for the three values of α_v: two limiting cases of accommodation and a third value of $\alpha_v = 0.8$ typical for NO molecules with high collision energies.[13] Again, if the distribution is considered for $\nu > 1$, the effective temperature is the same in all three cases (as well as for the curves shown in Fig. 9) and has an approximate value of 5000 K. For $\nu > 1$, all vibrational populations are higher when there is no accommodation with the wall, affecting the absolute magnitude of the IR spectra as well as its shape. The departure of the $\nu = 0$ and 1 levels from a Boltzmann distribution for $\alpha_v > 0$ illustrates that the majority of the NO at this spatial location has collided with the wall. The $\nu = 0$ level is increased relative to that of no accommodation because its energy value is closest to that of the 300-K wall.

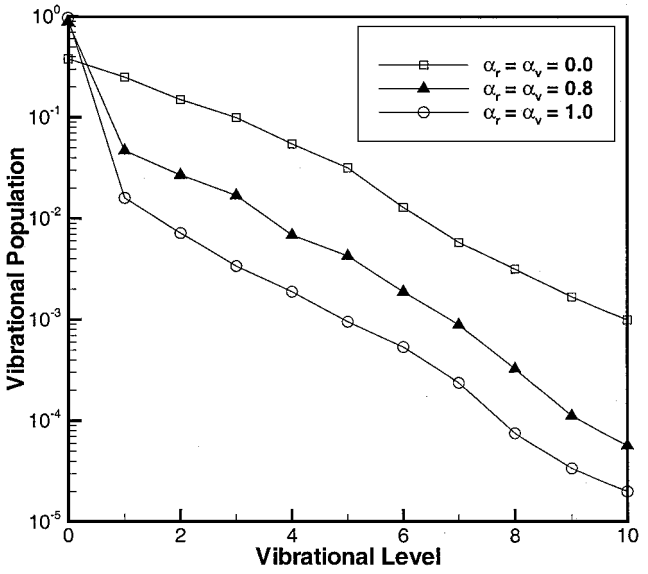

Fig. 10 Relative vibrational population distributions at $X = 0.1$ m along the LOS for $\alpha_v = 0$, 0.8, 1, and the QC data.

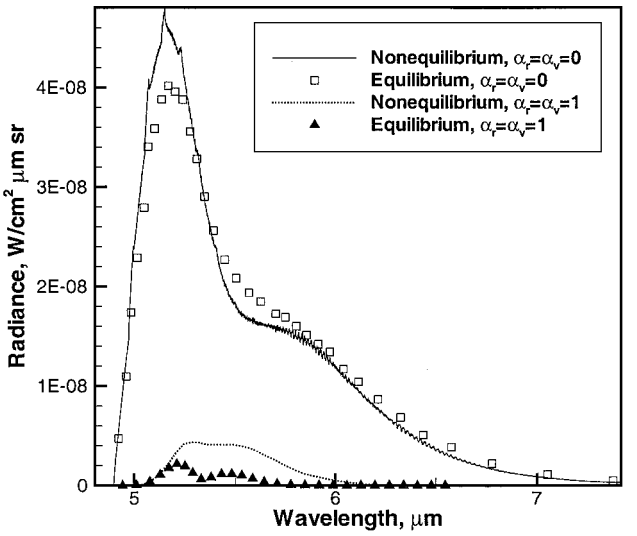

Fig. 11 Calculated spectra showing the NO IR fundamental transition $\Delta\nu = 1$ as a function of degree of accommodation and level of detail of vibrational distributions.

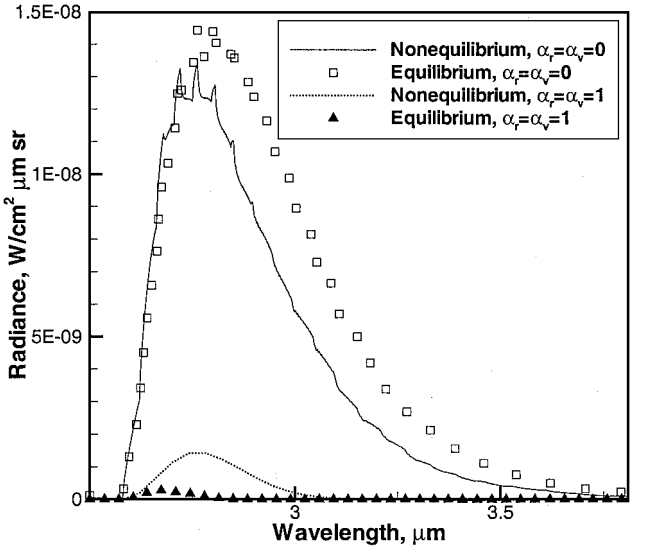

Fig. 12 Calculated spectra showing the NO IR overtone transition $\Delta\nu = 2$ and higher as a function of degree of accommodation and level of detail of vibrational distributions. The equilibrium, $\alpha_v = 1$, curve has been multiplied by a factor of 10.

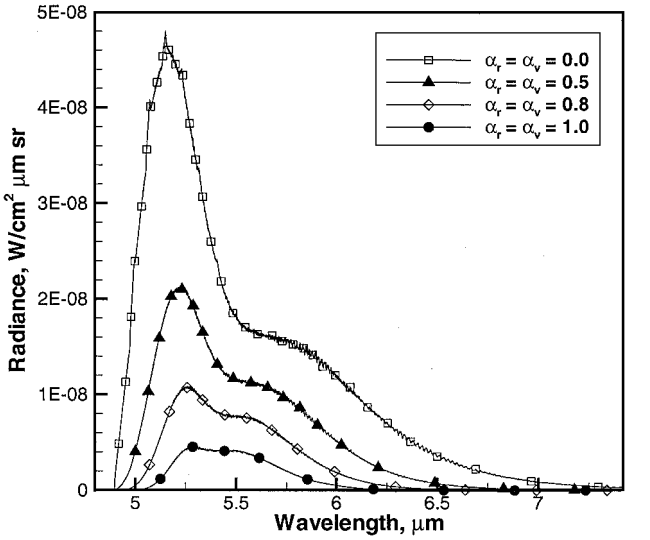

Fig. 13 Calculated spectra showing the NO IR fundamental transition $\Delta\nu = 1$ as a function of degree of accommodation for nonequilibrium populations.

The rotational temperatures are also affected by the degree of surface accommodation, or change in α_r. For $\alpha_r = 0$ the rotational temperature close to the surface is approximately 4400 K, whereas for $\alpha_r = 0.8$ it is ~1400 K.

Finally, spectra are calculated along the LOS of the SKIRT instrument using the NEQAIR-IR model for different wall accommodation values. All spectra are presented in units of spectral radiance (SR), watts per square centimeter micrometer steradian and are averaged over 600 Å. The most important feature of the spectra is the peak width and then the value of the peak height. A larger peak width indicates a higher NO vibrational temperature. Figures 11 and 12 show the calculated spectra in the NO fundamental and overtone spectral regions. Spectra are shown for the two limiting values of vibrational accommodation and two vibrational level population models. The models labeled nonequilibrium and equilibrium represent vibrational populations determined directly from the DSMC flow solution of the 21 nitric oxide vibrational states and a Boltzmann distribution at the NO vibrational temperatures [Eq. (5)]. The magnitude of the spectral radiance at a point in the flow is proportional to the number of NO molecules in each vibrational level. For a specific internal energy accommodation coefficient, the ratio between vibrational populations is similar at other locations along the stagnation line. Consistent with Fig. 10, the spectral radiance spatially integrated along the stagnation streamline for no accommodation ($\alpha_v = 0$) with the wall is approximately an order of magnitude higher than a fully accommodating wall ($\alpha_v = 1$). Also, the difference between the equilibrium and nonequilibrium spectra is larger for cases of full accommodation. Because a value of $\alpha_v = 0.8$ is more realistic than no accommodation, the nonequilibrium and equilibrium spectra for $\alpha_v = 1$ are of the most interest. If emphasis is given to these two spectra, it can be seen that the nonequilibrium spectrum gives a wider peak.

Figures 13 and 14 show simulated spectra in the fundamental and overtone bands, respectively, using the computed nonequilibrium vibrational populations as a function of the level of accommodation. In both spectral regions, the magnitude of the radiance increases with less accommodation of vibrational energy exchange with the cooler surface. More important, the shape of the spectra change because they are a composite of multiple vibrational level transitions. A nonaccommodating surface preserves the higher vibrational populations, which increases the contributions to the spectra at wavelengths longer than the band center peak. However, the level of nonaccommodation required to elevate the vibrational structure is physically unrealistic.

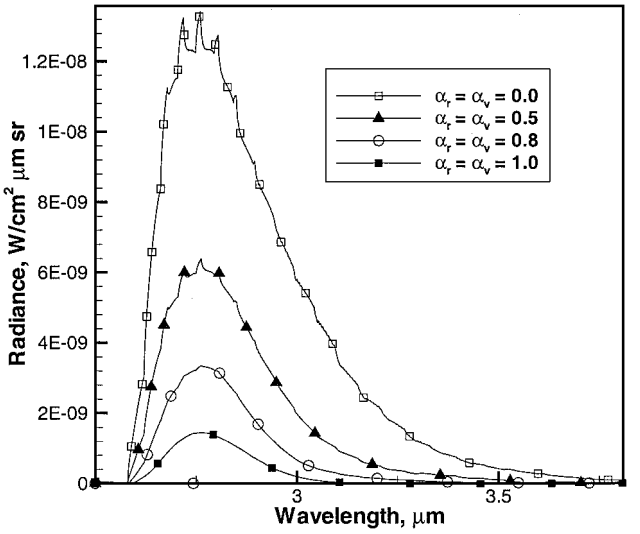

Fig. 14 Calculated spectra showing the NO IR overtone transition $\Delta\nu = 2$ and higher as a function of degree of accommodation for nonequilibrium populations.

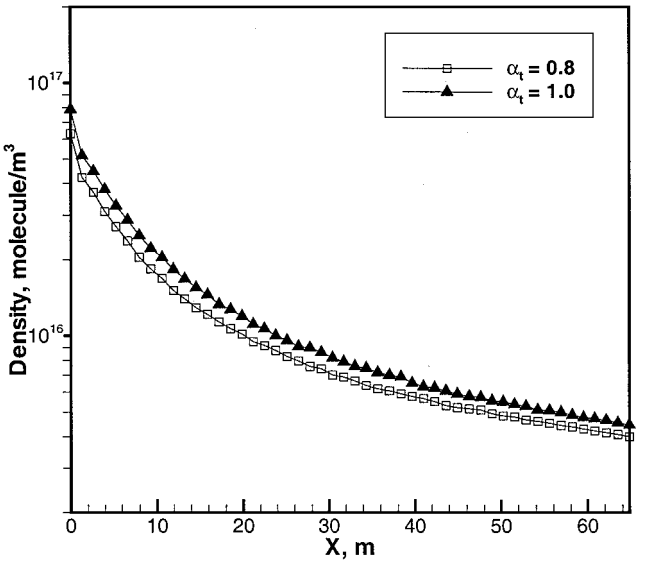

Fig. 15 Total number density along the LOS from the shuttle body to the freestream.

C. Sensitivity of Radiance to Translational Energy Accommodation Coefficient

In this section, the impact of the translational energy accommodation coefficient α_t on NO vibrational populations and spectra is examined. The results presented here were obtained using $\alpha_r = \alpha_v = 0.8$ and two values of α_t, 0.8 and 1. Surface reactions were neglected, and the postcollisional internal energy redistribution is given again by the Bose and Candler data.[15]

Figure 15 shows the total number density profiles along the LOS for two different values of α_t. Because 20% of particles reflect specularly for $\alpha_t = 0.8$ (i.e., with higher velocities than those reflected diffusely at 300 K), they move away faster from the body, which results in a reduced gas density of about 20%. Figure 16 shows that the translational temperature is also increased for $\alpha_t = 0.8$.

For $\alpha_t = 0.8$ there are more energetic collisions between the freestream O particles and the N_2 particles specularly reflected from the wall. The higher precollision relative energies in Eq. (1) causes a significant postcollisional energy redistribution toward higher vibrational levels. A comparison of the NO vibrational populations for the cases of $\alpha_t = 1$ and 0.8 is given in Fig. 17. The important point of Fig. 17 is that, for $\alpha_t = 0.8$, the slope of the upper vibrational levels changes so that the vibrational temperature based on these levels, for example, 7–10, approaches 8000 K. This value, in turn, agrees well with the estimate given in Ref. 12.

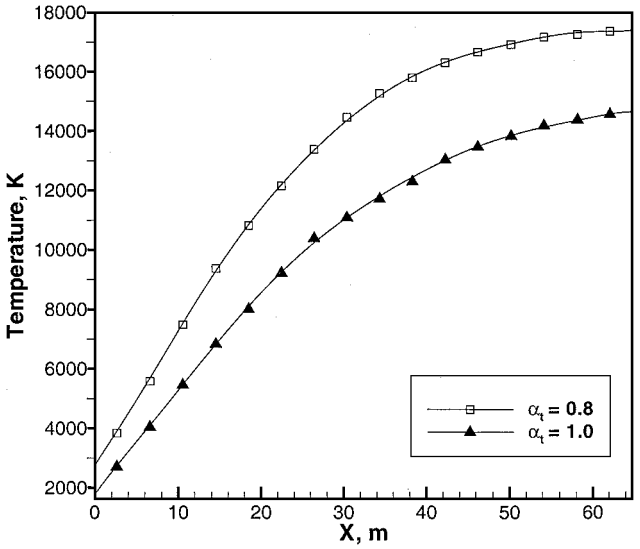

Fig. 16 Translational temperature profiles along the LOS from the shuttle body to the freestream.

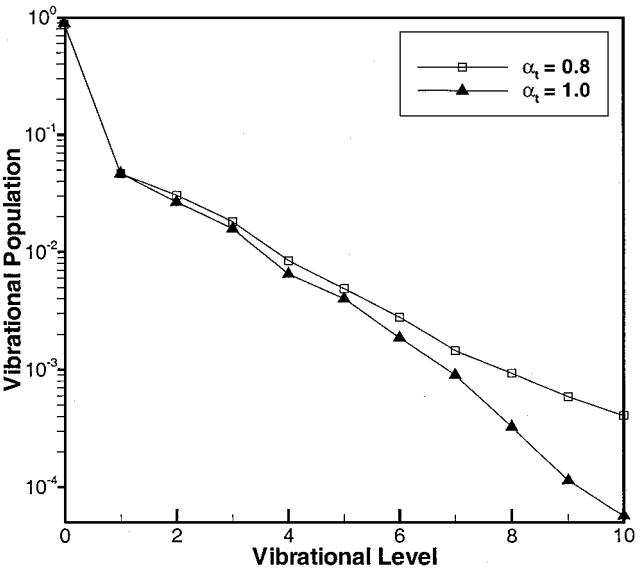

Fig. 17 Relative vibrational population distributions at $X = 0.1$ m along the LOS for $\alpha_t = 0.8$ and 1.0 and for the nonequilibrium model.

The larger populations of high vibrational levels for $\alpha_t = 0.8$ result in a considerably broader IR spectra. This is illustrated in Fig. 18, where the spectra are shown for the NO IR overtone transition. The spectra are close for the first five or six vibrational levels, whereas the radiance from higher vibrational levels $v > 10$ is significantly larger for $\alpha_t = 0.8$ (wavelength longer than 3 μm).

D. Impact of Surface Reactions and Surface Temperature

The results presented in the preceding sections were obtained using the Maxwell gas–surface interaction model with no surface reactions. Let us examine now the influence of the surface reactions on the formation of NO and the vibrational state distribution. Two sets of parameters that affect surface reactions were used (see Table 1 for their specific values). Figure 19 shows a comparison of the vibrational population distributions with and without surface reactions for $\alpha_t = 1$. Both surface models represent a potential depletion source of NO because they permit the conversion of NO to NO_2^*. In the surface models, incident NO gas can stick to the surface with a probability of 0.5, followed by subsequent desorption, conversion to NO_2^*, or ejection (by scrubbing) as NO. Ejected NO are assumed to accommodate to the 300-K surface in all modes. Because the sticking process effectively changes the internal energy accommodation coefficient, in the calculations presented in this section,

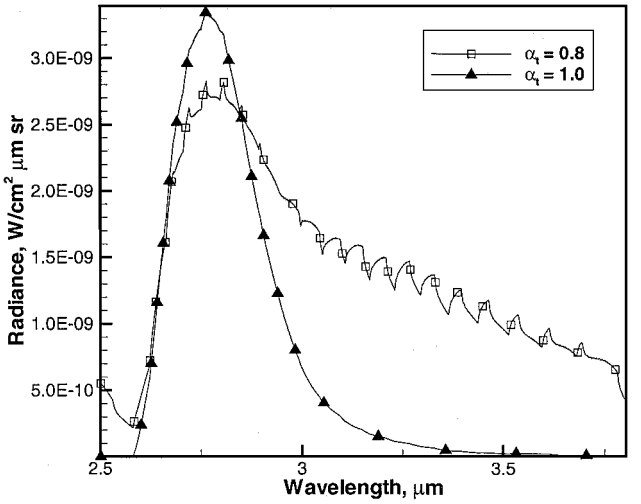

Fig. 18 Calculated spectra showing the NO IR overtone transition $\Delta\nu = 2$ and higher for $\alpha_t = 0.8$ and 1.0.

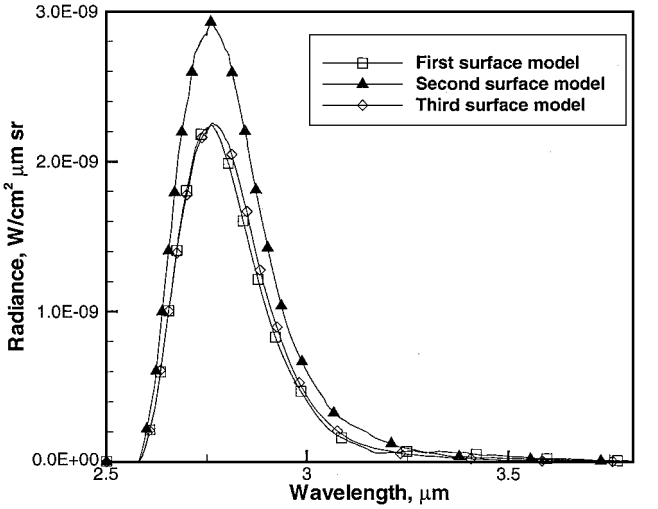

Fig. 20 Calculated spectra showing the NO IR overtone transition $\Delta\nu = 2$ for different surface models.

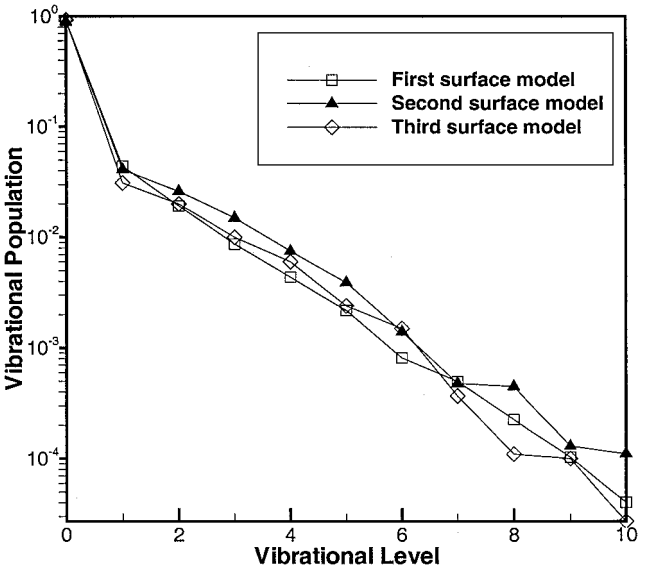

Fig. 19 Relative vibrational population distributions at $X = 0.1$ m along the LOS for the QC energy redistribution model and different surface models.

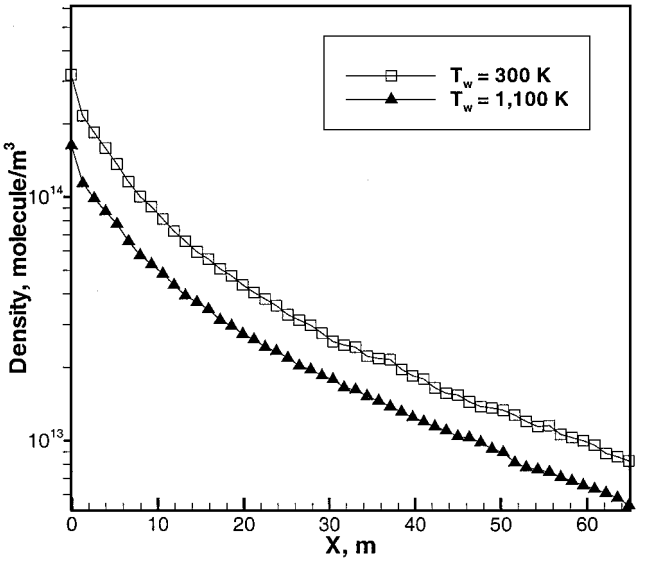

Fig. 21 Influence of the surface temperature on NO number density along the LOS from the shuttle body to the freestream; $\alpha_r = \alpha_v = 0.9$ and $\alpha_t = 1$.

$\alpha_r = \alpha_v$ was set to 0.8 and 0.9 for surface reactions turned on and off, respectively. This produces the same fraction of NO molecules reflected diffusely and, therefore, excludes the possible impact of α_v.

The surface reactions change the concentration of NO rather than the vibrational energies, and it is, therefore, not likely that the use of either surface model will significantly affect the vibrational populations, as can be seen in Fig. 19. Figure 20 shows that the magnitude of the radiation is slightly changed by the surface model but not the shape. As expected, the no-surface-reaction model predicts the highest amount of radiation. The main difference between the utilized surface models is the heat of adsorption. The higher heat of adsorption of the third model causes more NO to physisorb on the surface and represents a greater loss mechanism. Thus, the NO radiance shown in Fig. 20 for the third model is lower than the first. The differences among all three surface models are not large compared to other variations discussed earlier. Comparison of the NO IR spectra does not provide a way to discriminate the two surface models given in Table 1.

To examine the influence of the surface temperature that is often not well defined, the computations were conducted for two values of T_w, 300 and 1100 K. The latter value is probably an upper estimate for T_w. A higher surface temperature results in higher velocities of reflected particles. Under the rarefied conditions of 263 km, those higher velocities cause, in turn, a faster removal of reflected particles from the surface. The profiles of NO number density along the LOS are shown in Fig. 21. The number density near the surface for $T_w = 1100$ K is approximately one-half of that for $T_w = 300$ K due to the faster removal of molecules from the surface.

The almost four times larger wall temperature corresponds to almost two times larger velocities of reflected particles with an average velocity of 600 m/s for $T_w = 1100$ K. This value is still smaller than that of the freestream velocity of 8 km/s. As a result, the elevated surface temperature leads to some increase in the vibrational population of the upper levels, but the effect of increased surface temperature on IR spectra is not significant. The NO radiance is larger in the portion of the spectra connected with high vibrational levels for $T_w = 1100$ K (Fig. 22), whereas the position of the maximum is not changed.

E. Comparison with Experiment

The SKIRT instrument, having spectral coverage from 0.7 to 5.4 μm, was a cryogenically cooled circular variable filter instrument[11] that measured shuttle glow, airglow, and other phenomena. Similar instruments flew on shuttle missions STS-39 and 62. Figures 23–25 show the data taken by SKIRT, the species assignments of Ahmadjian et al.,[12] and simulated spectra based on the work presented here, for two angles of attack. In the measurements,[12]

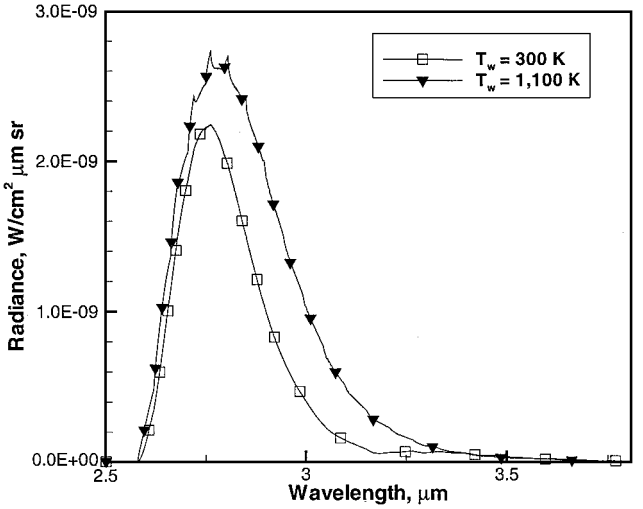

Fig. 22 Calculated spectra showing the NO IR overtone transition for two wall temperatures.

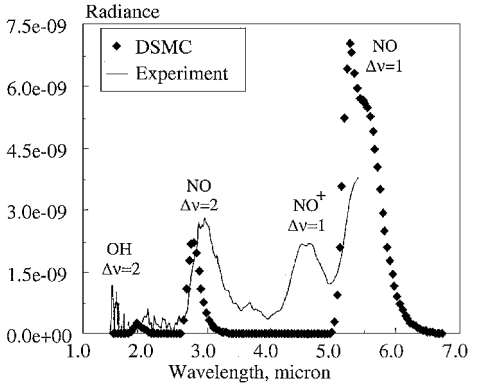

Fig. 23 Comparison of measured SKIRT and calculated spectra at zero angle of attack, $\alpha_t = 1.0$; SR is in watts per square centimeter micrometer steradian.

outgassing from external surfaces is believed to have been minimized, therefore reducing the possible contribution of other sources. In our calculations, the QC data, the third surface model, $\alpha_v = 0.8$, and $\alpha_t = 0.8$ and 1.0 values have been used. Our calculations did not include OH or NO^+ as potential IR sources. Note that, although NO_2 radiates in this spectral region, it is consistently not observed in the IR glow data. The level of NO irradiance is above the noise level of the instrument, and NO_2 is approximately $\frac{1}{10}$th of the NO population. Consistent with the data, the predicted level of radiation decreases for higher angle of attack.

For 0-deg angle of attack, there is a considerable difference observed in the widths of the predicted and experimental data for the $\Delta v = 2$ spectral region for $\alpha_t = 1$ (Fig. 23). The results of $\alpha_t = 1.0$ underpredict the data, whereas the calculation with $\alpha_t = 0.8$ overpredicts it. However, Fig. 24 shows that the calculated width of the NO $\Delta v = 2$ peak is in closer agreement to the experiment if a value of $\alpha_t = 0.8$ is assumed. Note that the vibrational temperature based on the upper levels for $\alpha_t = 0.8$ (Fig. 17) is close to 8000 K, similar to that obtained in Ref. 12. The location of the calculated peak in Figs. 23 and 24 is also different, 2.8 μm vs the value of 3.0 μm observed in the experiment. As shown in Fig. 25, the agreement is better for the angle of attack of 45 deg when $\alpha_t = 0.8$ is used. Generally, the experimental shape is reproduced well if a value of α_t between 0.8 and 1.0 is used. The improved agreement with experiment pertains to the comparison with both the width and the absolute value.

We also considered the possibility that there might be contributions from other radiating species, such as the OH fundamental. However, the source of the OH is not precisely defined, and, therefore, it is difficult to estimate its vibrational temperature, Moreover,

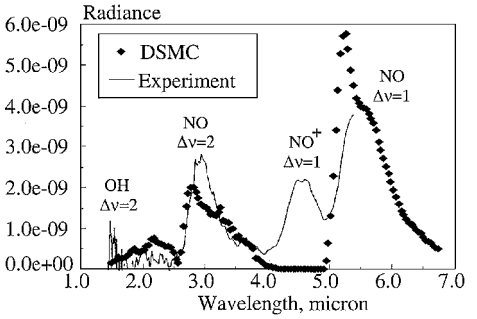

Fig. 24 Comparison of measured SKIRT and calculated spectra at zero angle of attack, $\alpha_t = 0.8$. SR is in watts per square centimeter micrometer steradian.

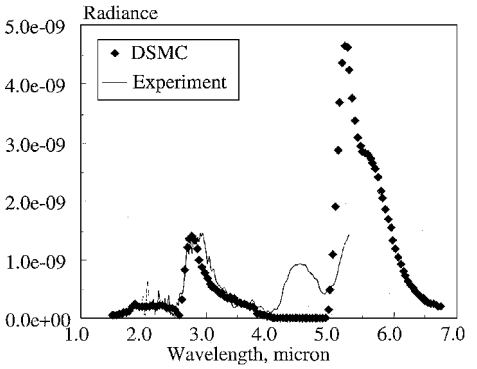

Fig. 25 Comparison of measured SKIRT and calculated spectra at 45-deg angle of attack, $\alpha_t = 0.8$.

for high vibrational temperatures, the OH fundamental and the overtone reverse in magnitude.

VI. Conclusions

The modeling of the IR radiation from nitric oxide produced in the flow about the space shuttle at 260 km was performed by the DSMC method using different gas–surface models. The radiation was calculated by the NEQAIR-IR code using the computed vibrational distributions. The work demonstrates the capability of the DSMC method to predict quantitatively radiative emission in the IR region in the rarefied, chemically reacting flows for low-Earth-orbital flight conditions. Several important specific conclusions may be drawn based on the results of the study.

Two different energy redistribution models were studied to analyze the products of the $N_2 + O \rightarrow NO + N$ reaction. The first model was taken from the QC data, and the second was an energy redistribution model based on the LB technique. Our work shows that the choice of energy redistribution model does not significantly impact the NO vibrational populations in the flow about the shuttle and consequently the NO IR spectra. The simple LB technique may, therefore, be used for this case where the vibrational distribution of reaction products is mostly equilibrium; this result, however, cannot be applied generally to other molecular systems.

The NO IR radiation was shown to be insensitive to the choice of surface chemistry model. Two different sets of surface parameters were used that account for absorption/desorption, glow, and scrubbing processes. Both sets gave similar NO vibrational populations and spectra. The radiance intensity was not found to be strongly dependent on the surface temperature either.

The influence of the internal (rotational and vibrational) energy accommodation coefficients was examined. The increase of the fraction of specularly reflected particles (i.e., particles whose internal energy does not change after a collision with the surface) causes an increase in the number of molecules with vibrational level higher than zero. The larger populations in the higher vibrational levels significantly increases the magnitude and slightly broadens the resultant NO spectra. The impact of the translational energy accommodation coefficient was also analyzed. It was shown that a decrease in

the translational accommodation coefficient considerably broadens the NO spectra while preserving the value of the maximum.

The steady-state solution for the level-specific NO vibrational populations in the DSMC modeling and its subsequent utilization in a radiation code, instead of a temperature-based approach, is critical for the accurate prediction of IR spectra. The impact of vibrational nonequilibrium is especially significant for internal energy accommodation coefficients close to one.

The comparison of the calculated spectra with the flight measurements was conducted. The agreement between the results of simulations and the experiment is quite satisfactory in the width of the spectra and especially in their maximum value (within 30% for 0-deg and 5% for 45-deg angle of attack) if the translational and internal energy accommodation coefficients of 0.8 are used. An assumption of 20% surface specularity is reasonable for both the velocities and vibrational energies of molecules in rarefied flow and is, therefore, recommended here. The increase in the number of particles whose velocities do not change after collisions with the surface causes a larger portion of collisions with greater energy. This, in turn, creates NO products with higher internal energy. This factor was found to be the most significant in reproducing the experimental data. It provides a fundamental explanation and confirmation of the NO vibrational temperature derived in the original analysis of Ahmadjian et al.[12] of the shuttle IR data.

Acknowledgments

The work at George Washington University and Pennsylvania State University was supported by Army Research Office Grant DAAG55-98-1-009 and Air Force Office of Scientific Research Grant F 49620-99-1-0143. We are grateful to the extra data provided to us by Deepak Bose of NASA Ames Research Center for the NO vibrationally resolved cross sections. We would also like to acknowledge the help of Christophe Laux at Stanford University in providing his NEQAIR-IR code and his assistance in modifying it as required for this work.

References

[1]Yee, J. H., and Abreu, V. J., "Visible Glow Induced by Spacecraft–Environment Interaction," *Geophysical Research Letters*, Vol. 10, No. 2, 1983, pp. 126–129.

[2]Swenson, G. R., Mende, S. B., and Clifton, K. S., "Ram Vehicle Glow Spectrum Implications of NO_2 Recombination Continuum," *Geophysical Research Letters*, Vol. 12, No. 2, 1985, pp. 97–100.

[3]Gimelshein, S. F., Levin, D. A., and Collins, R. J., "Modeling of Glow Radiation in the Rarefied Flow About an Orbiting Spacecraft," *Journal of Thermophysics and Heat Transfer*, Vol. 14, No. 4, 2000, pp. 471–479.

[4]Gimelshein, S. F., Collins, R. J., and Levin, D. A., "Numerical Modeling of Radiation in Flows About a Reentry Vehicle at High Altitudes," *Proceedings of the 22nd International Symposium on Shock Waves*, edited by G. J. Ball, R. Hiller, and G. T. Roberts, Vol. 1, Univ. of Southampton, Southampton, England, U.K., 2000, pp. 763–768.

[5]Collins, R. J., Levin, D. A., and Dogra, V. K., "A Reexamination of the Atmospheric Explorer Data Using the DSMC Technique," *Proceedings of the 20th International Symposium on Gas Dynamics*, edited by R. Brun, R. Gatinol, and J. C. Lengrand, Vol. 1, Cepadues Editions, Toulouse, France, 1999, pp. 665–672.

[6]Murad, E., "The Shuttle Glow Phenomenon," *Annual Review of Physical Chemistry*, Vol. 49, 1998, pp 73–98.

[7]Gasser, R. P. H., *An Introduction to Chemisorption and Catalysis by Metals*, Clarendon, Oxford, 1985, pp. 196, 197.

[8]Karipides, D. P., Boyd, I. D., and Caledonia, G. E., "Development of a Monte Carlo Overlay Method with Application to Spacecraft Glow," *Journal of Thermophysics and Heat Transfer*, Vol. 12, No. 1, 1998, pp. 30–37.

[9]Gimelshein, S. F., Levin, D. A., and Collins, R. J., "Modeling of Infrared Radiation in a Space Transportation System Environment," AIAA Paper 2000-0731, 2000.

[10]Swenson, G. R., Rairden, R. L., Jennings, D. E., and Ahmadjian, M., "Vehicle Glow Measurements on Space Transportation System Flight 62," *Journal of Spacecraft and Rockets*, Vol. 33, No. 2, 1995, p. 240.

[11]Ahmadjian, M., and Jennings, D., "Analysis of STS-39 Space Shuttle Glow Measurements," *Journal of Spacecraft and Rockets*, Vol. 32, No. 3, 1995, pp. 507–513.

[12]Ahmadjian, M., Jennings, D., Mumma, M., Espenak, F., Rice, C., Russell, R., and Green, B., "Infrared Spectral Measurement of Space Shuttle Glow," *Geophysical Research Letters*, Vol. 19, No. 10, 1992, pp. 989–992.

[13]Asscher, M., Guthrie, W. L., Lin, T.-H., and Somorjai, G. A., "Energy Redistribution Among Internal States of Nitric Oxide Molecules upon Scattering from Pt(111) Crystal Surface," *Journal of Chemical Physics*, Vol. 78, No. 11, 1983, pp. 6992–7004.

[14]Bird, G. A., *Molecular Gas Dynamics and the Direct Simulation of Gas Flows*, Clarendon, Oxford, 1994, pp. 208–256.

[15]Bose, D., and Candler, G. V., "Kinetics of the $N_2 + O \leftarrow NO + N$ Reaction Under Thermodynamic Nonequilibrium," *Journal of Thermophysics and Heat Transfer*, Vol. 10, No. 1, 1996, p. 148.

[16]Borgnakke, C., and Larsen, P. S., "Statistical Collision Model for Monte Carlo Simulation of Polyatomic Gas Mixture," *Journal of Computational Physics*, Vol. 18, No. 4, 1975, pp. 405–420.

[17]Haas, B., "Models of Energy-Exchange Mechanics Applicable to a Particle Simulation of Reactive Flow," *Journal of Thermophysics and Heat Transfer*, Vol. 6, No. 2, 1992, pp. 200–207.

[18]Ivanov, M. S., Markelov, G. N., and Gimelshein, S. F., "Statistical Simulation of Reactive Rarefied Flows: Numerical Approach and Applications," AIAA Paper 98-2669, June 1998.

[19]Ivanov, M. S., and Rogasinsky, S. V., "Analysis of the Numerical Techniques of the Direct Simulation Monte Carlo Method in the Rarefied Gas Dynamics," *Soviet Journal of Numerical Analysis and Mathematical Modeling*, Vol. 3, No. 6, 1988, pp. 453–465.

[20]Packan, D. M., Gessman, R. J., Pierrot, L., Laux, C. O., and Kruger, C. H., "Measurement and Modeling of OH, NO, and CO_2 Infrared Radiation in a Low-Temperature Air Plasma," AIAA Paper 99-3605, 1999.

[21]Boyd, I. D., Bose, D., and Candler, G. V., "Monte Carlo Modeling of Nitric Oxide Formation Based on Quasiclassical Trajectory Calculations," *Physics of Fluids*, Vol. 9, No. 4, 1997, pp. 1162–1170.

J. P. Gore
Associate Editor